

Colloid aggregation induced by oppositely charged polyions

Ludger Harnau^{1,2} and Jean-Pierre Hansen³

¹*Max-Planck-Institut für Metallforschung, Heisenbergstr. 1, D-70569 Stuttgart (Germany)*

²*Institut für Theoretische und Angewandte Physik, Universität Stuttgart, Pfaffenwaldring 57, D-70569 Stuttgart (Germany)*

³*Department of Chemistry, University of Cambridge, Lensfield Road, Cambridge CB2 1EW (UK)*

(March 16, 2022)

The "polymer reference interaction site model" (PRISM) integral equation formalism is used to determine the pair structure of binary colloidal dispersions involving large and small polyions of opposite charge. Two examples of such bidisperse suspensions are considered in detail, namely mixtures of charged spherical colloids and oppositely charged polyelectrolyte chains, and binary mixtures of oppositely charged large and small clay platelets. In both cases clear evidence is found for aggregation of the larger particles induced by the polyionic counterions, signalled by a strong enhancement of long wavelength concentration fluctuations.

I. INTRODUCTION

In metallurgy it has been known for several millenia that mechanical properties of many metals can be considerably improved by alloying two or several elements. Similar improvements of material properties of "soft matter" can be achieved by mixing two or more macromolecular components in fluid solutions or dispersions. One of the oldest known examples is the stabilization of colloidal suspensions by the addition of adsorbing polymer, which was already used in ancient Egypt for the preparation of inks. On the contrary, flocculation of colloids can be driven by the addition of non-adsorbing polymer via the depletion mechanism¹. More recent is the realization of the key role of Coulombic interactions in determining and improving material or physiological properties of complex colloidal and biomolecular systems, and their exploitation in numerous technological and biomedical applications. Widely studied systems include suspensions of charged colloids and polyelectrolytes^{2,3}, polymer-clay nanocomposites⁴ or DNA bundles and DNA-lipid complexes⁵. For example, even small polyelectrolyte additives can have a substantial impact on the aggregation and kinetic stability of charged colloidal particles³. On the other hand, just a small fraction of clay fillers doubles the tensile strength of a polymer matrix⁶, while highly asymmetric mixtures of charged clay platelets are used to improve rheological properties of drilling fluids⁷.

To design complex mixtures with optimal properties, it is essential to gain a quantitative understanding of correlations and effective interactions between various macromolecular species. This can be achieved using the well-established techniques of liquid-state theory⁸. The PRISM ("polymer reference interaction site model") theory, originally designed for the study of polymer solutions and melts⁹, has been recently extended to investigate various charged and uncharged colloidal systems^{10,11}, as well as mixtures of neutral spherical colloids and polymers^{12–15} and like-charged spherical colloids and polyelectrolytes¹⁶.

This paper focuses on the structure and stability of dispersions of charged colloidal particles in the presence

of oppositely charged polyions, which play the role of mesoscopic counterions. There is a considerable literature on the widely studied case of microscopic counterions and the resulting effective interactions between the highly charged colloidal particles¹⁷. In particular, it is now well established that divalent counterions can lead to overscreening of the Coulombic interaction between spherical or rod-like colloidal particles, which results in a correlation-induced, short-range attraction between the latter^{18–20}. The case where the counterions are mesoscopic or macromolecular polyions has received much less attention so far, except for the simplest case of polyelectrolyte chains confined between two infinite parallel plates carrying charges of opposite sign to the polyelectrolyte, where overcompensation of the charge on the platelets, leading to effective attraction between the latter, has been predicted^{21,22}.

Two systems involving mesoscopic counterions are examined in the present paper, namely a) mixtures of highly charged spherical colloids and oppositely charged polyelectrolyte chains and b) binary mixtures of oppositely charged platelets of widely different diameters. The key problem to be addressed is that of structural diagnostics of a possible aggregation of the larger particles induced by the smaller particles, over a range of physical conditions. This goal is achieved by determining pair correlation functions and partial structure factors within the framework of PRISM, which is adapted in this paper to the systems in hand.

II. INTERACTION SITE MODELS

The two systems under investigation are aqueous dispersions or solutions, but in view of the mesoscopic scale of the particles, the solvent will be modelled as a structureless dielectric continuum providing a macroscopic permittivity ϵ . Any microscopic counterions or ions from added electrolyte will be considered at the linear response (or Debye-Hückel) level, i.e., they will screen the electrostatic potential due to the interaction sites on the colloids or polyions on a scale given by the usual Debye screen-

ing length λ_D ²³. The underlying Born-Oppenheimer-like assumption entails that the charge distribution on the mesoscopic particles does not contribute to screening²⁴. Since sites with charge of opposite sign are involved, the site-site interaction must contain a short-range repulsion, which will be modelled by hard sphere (HS) cores of diameter d_i . The interaction potential between sites on particles of species i and j , carrying the charges $z_i e$ and $z_j e$, will hence be of the generic form:

$$u_{ij}(r) = \begin{cases} \infty, & r \leq \frac{1}{2}(d_i + d_j), \\ \frac{z_i z_j e^2}{\epsilon r} \exp(-\kappa_D r), & r > \frac{1}{2}(d_i + d_j), \end{cases} \quad (2.1)$$

where $\kappa_D = \lambda_D^{-1}$. On the polyelectrolyte, N_p charged sites are distributed at regular intervals along the linear macromolecular backbone, each site being associated with a monomer or segment of diameter d_p . The clay platelets will be modelled as circular discs of radius R , carrying interaction sites uniformly distributed on the surface; the core diameter associated with these sites accounts for the finite thickness of the platelets. As regards the spherical colloids, two models may be considered. In model A, N_s charged sites are distributed over the spherical surface of radius R . For a sufficiently large density $N_s/(4\pi R^2)$ of the surface sites, the hard cores of diameter d_s associated with each site will ensure that the spheres are impenetrable. In model B, the impenetrability of the spherical colloids is ensured by an uncharged central (c) site, with a core radius identical to the particle radius, while the electrostatic interactions are carried by N_s surface sites distributed on a spherical shell of radius $R - d_s/2$. Each surface site carries a charge equal to the total charge on the colloid divided by the number of sites. Invoking Gauss' theorem, it might be argued that this distribution should be equivalent to a single site carrying the full colloidal charge at the centre of the sphere. This equivalence would hold within an exact theory, but since an approximate closure relation is to be used, as discussed in section III, more accurate results may be expected when interaction sites with lower charges are used, such that the Coulomb coupling is weaker.

Within the PRISM formalism to be discussed in the next section, all interaction sites of the same type (i.e., p , c , or s) are assumed to be equivalent, leading to a considerable simplification over the original RISM²⁵. This assumption is obviously exact for spherical particles with surface sites only (model A), but is an approximation for polyelectrolytes of finite length (since end effects are neglected), and even more so for platelets, where edge effects are not taken into consideration. However previous experience with neutral or charged rods¹⁰ and platelets¹¹ shows that the basic PRISM assumption does lead to sensible results for the pair structure of these rigid particles.

III. MULTICOMPONENT PRISM

Consider a multicomponent system involving ν species of particles with number densities ρ_α ($1 \leq \alpha \leq \nu$), each particle of a species involving n_α classes of exactly or approximately equivalent interaction sites. The total number of distinct classes of sites in the mixture is

$$\sum_{\alpha=1}^{\nu} n_\alpha = N. \quad (3.1)$$

It proves convenient to assign an index i ($1 \leq i \leq N$) to each class of sites, and to order them such that classes $1 \leq i \leq n_1$ belong to particles of species 1, classes $n_1+1 \leq i \leq n_1+n_2$ belong to species 2, ..., and classes $N-n_\nu \leq i \leq N$ belong to species ν . Each class i contains N_i equivalent interaction sites, and if the positions of sites belonging to classes i and j are designated by $\mathbf{r}_k \equiv \mathbf{r}_k^{(i)}$, and $\mathbf{r}_l \equiv \mathbf{r}_l^{(j)}$ ($1 \leq k \leq N_i$; $1 \leq l \leq N_j$), then one may define the usual intramolecular structure factors, or form factors

$$\omega_{ij}(\mathbf{q}) = \frac{1}{\sqrt{N_i N_j}} \sum_{k=1}^{N_i} \sum_{l=1}^{N_j} \left\langle e^{i\mathbf{q} \cdot (\mathbf{r}_k - \mathbf{r}_l)} \right\rangle \quad (3.2)$$

provided i and j sites belong to the same particle, while $\omega_{ij}(\mathbf{q}) \equiv 0$ otherwise. The $\omega_{ij}(\mathbf{q})$ are hence elements of a $N \times N$ box-diagonal matrix $\boldsymbol{\omega}(\mathbf{q})$. In the present paper *rigid* platelets and spherical colloids are considered, so that

$$\omega_{ij}(q) = \delta_{ij} + \frac{1}{\sqrt{N_i N_j}} \sum_{k=1}^{N_i} \sum_{l=1}^{N_j'} \frac{\sin(qr_{kl})}{qr_{kl}}, \quad (3.3)$$

where $r_{kl} = |\mathbf{r}_k - \mathbf{r}_l|$, $q = |\mathbf{q}|$, and the prime signifies that the "self" term $k = l$ is to be left out for the diagonal elements $i = j$. PRISM is based on the assumption that all direct correlation functions between sites on pairs of different particles are identical if these sites belong to the same class on each of the two particles. This leaves a total of $N(N+1)/2$ independent direct correlation functions $c_{ij}(q)$. Corresponding total correlation functions $h_{ij}(q)$ are defined by averaging over the $N_i N_j$ correlation functions between all pairs of equivalent sites belonging to classes i and j on two particles of the same or different species. The $N \times N$ matrices of $c_{ij}(q)$ or $h_{ij}(q)$ are symmetric, but it proves convenient to introduce auxiliary non-symmetric matrices $\mathbf{H}(q)$, $\mathbf{C}(q)$ and $\mathbf{W}(q)$, with elements

$$H_{ij}(q) = \rho_i N_i N_j h_{ij}(q), \quad C_{ij}(q) = \rho_i c_{ij}(q), \quad (3.4)$$

$$W_{ij}(q) = \sqrt{N_i N_j} \omega_{ij}(q), \quad (3.5)$$

where ρ_i is the number density of that species of particles to which sites of category i belong. With these conventions, the set of $N(N+1)/2$ Ornstein-Zernike (OZ) relations can be cast in the compact form^{10,25,26}

$$\mathbf{H}(q) = \mathbf{W}(q)\mathbf{C}(q)[\mathbf{W}(q) + \mathbf{H}(q)] \quad (3.6)$$

which may be solved for $\mathbf{H}(q)$ according to:

$$\mathbf{H}(q) = ([\mathbf{I} - \mathbf{W}(q)\mathbf{C}(q)]^{-1} - \mathbf{I}) \mathbf{W}(q). \quad (3.7)$$

The set of $N(N+1)/2$ independent OZ relations must be supplemented by as many closure relations between each pair of total and direct correlation functions. For intersite distances $r > d_{ij} = (d_i + d_j)/2$, we adopt the partially linearized Laria-Wu-Chandler closure^{27,28}:

$$\begin{aligned} & \frac{h_{ij}(r) + 1}{h_{ij}^0(r) + 1} \exp[h_{ij}^0(r) - \omega_{ii} * c_{ij}^0 * \omega_{jj}(r)] \\ &= \begin{cases} \exp[\chi_{ij}(r)], & \chi_{ij}(r) \leq 0 \\ 1 + \chi_{ij}(r), & \chi_{ij}(r) > 0, \end{cases} \end{aligned} \quad (3.8)$$

with

$$\chi_{ij}(r) = h_{ij}(r) - \omega_{ii} * (\beta u_{ij} + c_{ij}) * \omega_{jj}(r), \quad (3.9)$$

where $\beta = 1/(k_B T)$ is the inverse temperature. The superscript 0 refers to the underlying reference model with hard core interactions only (i.e., without the screened Coulomb interaction in Eq. (2.1)), while the asterisk $*$ denotes a convolution product. The reference site-site correlation functions $c_{ij}^0(r)$ and $h_{ij}^0(r)$ are obtained by solving the set of OZ equations (3.6) with the atomic Percus-Yevick closure for hard spheres, i.e. $h_{ij}^0(r) = -1$, $r \leq d_{ij}$; $c_{ij}^0(r) = 0$, $r > d_{ij}$ ⁸. The closure (3.8) takes the long-range asymptotics of the direct correlation functions $c_{ij}(r)$, in terms of the molecular hypernetted chain (HNC) approximation^{8,25}, into account, but prevents the exponential increase of the total correlation functions $h_{ij}(r)$ for distances corresponding to strong attraction between oppositely charged sites²⁹. By construction, the total correlation functions and their first derivatives are continuous when $\chi_{ij}(r) = 0$.

The closed set of equations (3.7) - (3.9) are solved numerically by a standard iterative procedure to obtain pair distribution functions $g_{ij}(r) = 1 + h_{ij}(r)$, and partial structure factors:

$$S_{ij}(q) = \omega_{ij}(q)\delta_{ij} + \rho_i h_{ij}(q). \quad (3.10)$$

IV. COLLOID-POLYELECTROLYTE MIXTURES

In this binary mixture ($\nu = 2$), species 1, referred to with the index p , are semiflexible polyelectrolyte chains with N_p equivalent segments carrying each a charge $z_p e = Z_p e/N_p$ (where $Z_p e$ is the total charge of each chain). The form factor of the semiflexible chain is³⁰:

$$\begin{aligned} \omega_p(q) &= 1 + \frac{2}{N_p} \sum_{n=1}^{N_p-1} (N_p - n) \\ &\times \exp \left[-\frac{q^2}{3} [n d_p l_p - l_p^2 (1 - e^{-n d_p / l_p})] \right], \end{aligned} \quad (4.1)$$

where d_p is the segment length and l_p is the persistence length. The spherical colloids of radius R_c (species 2), carry two categories of sites: N_s rigidly arranged surface sites of diameter d_s carrying an electric charge $z_s e = Z_c e/N_s$ (where $Z_c e$ is the total charge of each colloidal particle), and one central site, labelled with the index c , which is non-interacting (model A), or the centre of a hard sphere repulsion of radius R_c (model B). In this paper only calculations based on model A will be presented. The corresponding form factors are $\omega_{cc}(q) = 1$,

$$\omega_{ss}(q) = 1 + N_s \left(\frac{\sin(q R_c)}{q R_c} \right)^2, \quad (4.2)$$

$$\omega_{cs}(q) = \sqrt{N_s} \frac{\sin(q R_c)}{q R_c}, \quad (4.3)$$

where the double sums in Eq. (3.3) have been replaced by double integrals corresponding to a continuous distribution of interaction sites on the surface of the sphere of radius R_c . Since this corresponds formally to the limit $N_s \rightarrow \infty$, the two form factors (4.2) and (4.3) are approximately related by $\omega_{ss}(q) = \omega_{cs}^2(q)$. In practical calculations $N_s = 60$ was chosen. If no microscopic co- and counterions are present, charge neutrality relates the polyelectrolyte and colloid density via:

$$Z_c \rho_c + Z_p \rho_p = 0. \quad (4.4)$$

In the absence of microscopic ions, $\kappa_D = 0$, and the potentials $u_{ij}(r)$ in Eq. (2.1) reduce to bare Coulomb potentials. With three classes of sites (p , s and c), the matrix $\mathbf{W}(q)$ is given by:

$$\mathbf{W}(q) = \begin{pmatrix} \omega_{pp}(q) & 0 & 0 \\ 0 & \omega_{ss}(q) & \omega_{cs}(q) \\ 0 & \omega_{cs}(q) & \omega_{cc}(q) \end{pmatrix}. \quad (4.5)$$

There are a priori 6 independent direct and total correlation functions $c_{ij}(q)$ and $h_{ij}(q)$ ($i, j = p, s$ or c). However, independently of any specific closure relation, the OZ equations lead directly to the following three relations between the total correlation functions:

$$h_{ss}(q) = \omega_{cs}^2(q) h_{cc}(q), \quad (4.6)$$

$$h_{cs}(q) = \omega_{cs}(q) h_{cc}(q), \quad (4.7)$$

$$h_{ps}(q) = \omega_{cs}(q) h_{pc}(q). \quad (4.8)$$

These relations reflect the fact that the "free-rotation" approximation⁸ for rigid molecules is in fact exact when the interaction sites are distributed on the surface of a sphere. Other decoupling schemes which have recently been put forward for polymeric systems^{31,32} are also exact in that limit.

We have considered mixtures of colloids of radius $R_c = 150$ nm, and of oppositely charged semiflexible polyelectrolyte chains of contour length $L = 600$ nm and persistence length $l_p = 25$ and 50 nm in water at room temperature ($e^2/(\epsilon k_B T) = 0.714$ nm).

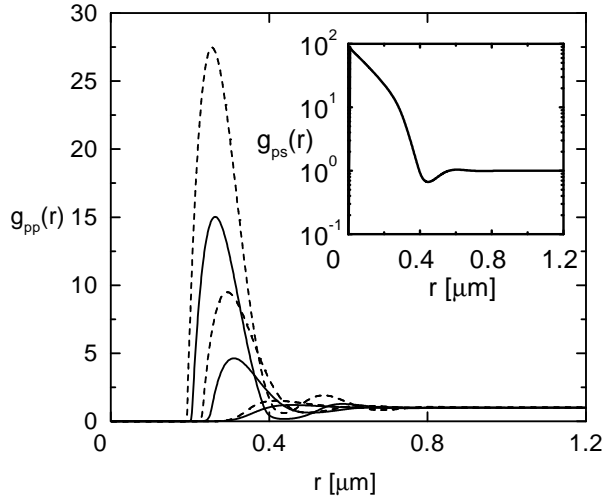


FIG. 1. Polyelectrolyte pair correlation function $g_{pp}(r)$ for a mixture of semiflexible polyelectrolytes (contour length $L = 600$ nm) and oppositely charged spherical colloids (radius $R_c = 150$ nm) for various valences $Z_p = -Z_c = 200, 400, 600$ (from bottom to top) at $\rho_c = 0.5 \mu\text{m}^{-3}$. The solid and dashed lines are calculated using the persistence length $l_p = 100$ nm and $l_p = 50$ nm, respectively. The inset displays the polyelectrolyte-colloid surface site correlation function $g_{ps}(r)$ for $Z_c = -Z_p = 400$ and $l_p = 100$ nm.

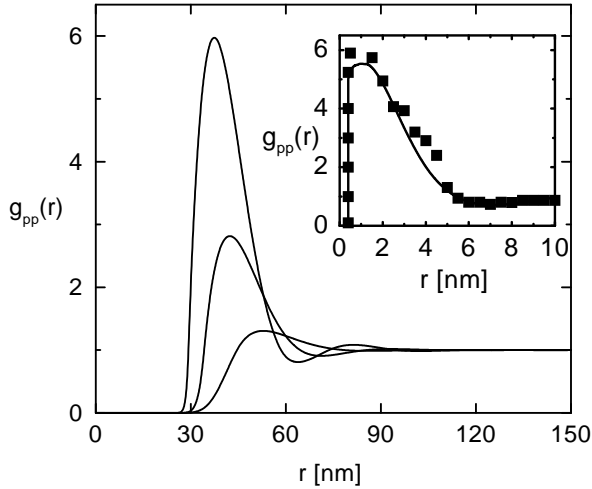


FIG. 2. Polyelectrolyte pair correlation function $g_{pp}(r)$ for a mixture of semiflexible polyelectrolytes (contour length $L = 60$ nm, persistence length $l_p = 10$ nm) and oppositely charged spherical colloids (radius $R_c = 20$ nm) for various valences $Z_p = -Z_c = 50, 75, 100$ (from bottom to top) at $\rho_c = 5 \times 10^{-7} \text{nm}^{-3}$. The inset displays $g_{pp}(r)$ for a mixture of charged dimers ($L = 1$ nm) and oppositely charged small spherical particles ($R_c = 2$ nm) for $Z_c = -60$ together with computer simulation data (squares)³³.

The calculated pair distribution functions $g_{pp}(r)$ are shown in Fig. 1 for three values of Z_c . The interchain cor-

relations are seen to increase dramatically with Z_c , and to be much more pronounced for the more flexible chains. Qualitatively similar results hold for a mixture involving smaller colloidal particles and shorter chains, as shown in Fig. 2. The reliability of PRISM is illustrated in the inset of that Figure, where the PRISM predictions for $g_{pp}(r)$ is compared to available Monte Carlo data³³ for a mixture of charged spheres and oppositely charged dimers. The unusually large amplitude of the first peak in $g_{pp}(r)$ is the signature of an enhanced polyelectrolyte density near the oppositely charged spherical colloids, reminiscent of the well-known "counterion condensation" of small ions^{34,35}. This condensation may drive phase separation³³ which can be diagnosed by large fluctuations in the colloid density.

Examples of the colloid centre of mass structure factor $S_{cc}(q)$ are shown in Fig. 3. A central peak in the $q \rightarrow 0$ limit is seen to build up as the colloid density ρ_c increases. The enhancement of the density fluctuations, as characterized by $S_{cc}(q = 0)$, is illustrated in Fig. 4, as a function of ρ_c for several values of Z_c . Although no divergence occurs, the tendency towards segregation is clear. In a naive random phase approximation (RPA) picture, values of $S_{cc}(0) > 1$ point to an effective long range attraction between the colloidal particles. The existence of an attraction between the colloidal particles, induced by the oppositely charged polyelectrolyte, can be more firmly established by a direct inversion of the pair distribution function $g_{ss}(r)$ of surface sites on the colloids.

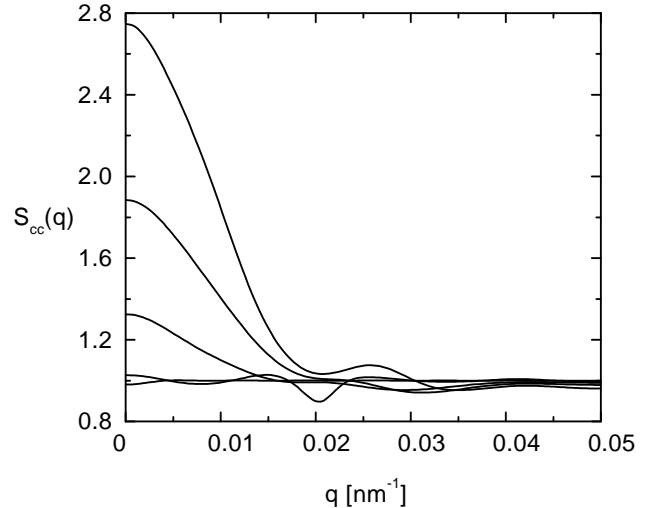


FIG. 3. Colloid centre of mass structure factor $S_{cc}(q)$ for a mixture of semiflexible polyelectrolytes ($L = 600$ nm, $l_p = 50$ nm) and oppositely charged spherical colloids ($R_c = 150$ nm, $Z_c = 1000$, $Z_p = -800$) for various densities $\rho_c = 0.004, 0.04, 0.1, 0.2, 0.4 \mu\text{m}^{-3}$ (from bottom to top).

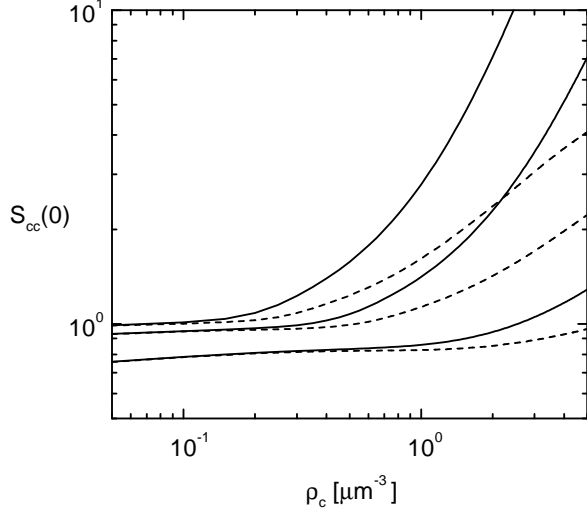


FIG. 4. Colloid centre of mass structure factor at zero scattering vector $S_{cc}(0)$ as a function of colloid density, for a mixture of semiflexible polyelectrolytes ($L = 600$ nm) and oppositely charged spherical colloids ($R_c = 150$ nm) for various valences $Z_c = -Z_p = 100, 200, 300$ (from bottom to top). The solid and dashed lines are calculated using the persistence length $l_p = 25$ nm and $l_p = 50$ nm, respectively.

In the limit $\rho_c \rightarrow 0$, this effective potential between surface sites would coincide with the potential of mean force, $v_{ss}(r) = -k_B T \log g_{ss}(r)$, but at finite concentration of colloids, an inversion based on an accurate closure relation must be used. In other words the inverse problem is solved, whereby the pair distribution function $g_{ss}(r)$, as calculated from the solution of the multicomponent PRISM equations, is known, and the effective potential $v_{ss}(r)$ is extracted from the one-component version of the theory, using the corresponding one-component OZ and closure relations. Note that the inversion does not require an iterative procedure. Similar inversions have recently been successfully used to determine effective interactions between the centres of mass of interacting polymer coils³⁶, and between the interaction sites of rodlike polyelectrolytes³⁷.

Examples of the effective potentials are shown Fig. 5. As the charge $Z_c e$ increases, an attractive well develops and deepens. Instability towards colloid clustering and genuine phase separation is expected to occur when the well-depth becomes of the order $k_B T$, so that yet stronger Coulomb interaction, i.e., more highly charged polyelectrolyte, would be needed to drive the phase separation. This is presently under investigation. A comparison with the bare Coulomb interaction (2.1) clearly demonstrates the enhanced screening effect of the polyelectrolyte as the charge increases. The same figure also shows the effective potential $v_{cc}(r)$ between the centres of the colloidal particles, obtained from an HNC inversion of the centre to centre pair distribution function $g_{cc}(r)$ for one value of Z_c .

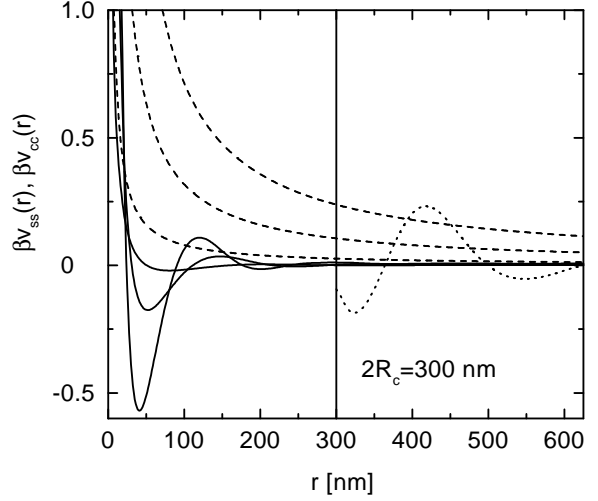


FIG. 5. Effective potential between surface sites on neighbouring colloids (solid line), and the bare Coulomb site-site interaction (dashed line) for a mixture of charged spherical colloids (radius $R_c = 150$ nm) in the presence of oppositely charged polyelectrolytes (contour length $L = 600$ nm, persistence length $l_p = 50$ nm) at $\rho_c = 5 \mu\text{m}^{-3}$. From top to bottom the solid lines correspond to increasing values of valences ($Z_c = -Z_p = 200, 400, 600$), while the dashed lines correspond to decreasing values of Z_c . The dotted line represents the effective potential $v_{cc}(r)$ between the centres of the colloidal particles as derived from an HNC inversion of $g_{cc}(r)$ for $Z_c = -Z_p = 200$.

V. BIDISPERSE CLAY SUSPENSIONS

We now turn to binary mixtures of oppositely charged disc-shaped platelets of different radii, R_1 and R_2 suspended in water, in the presence of microscopic co- and counterions. N_1 and N_2 interaction sites are assumed to be uniformly distributed over the surfaces of the discs of species 1 and 2, and interact via the screened Coulomb potential (2.1); the hard core diameters d_1 and d_2 determine the effective thickness of the platelets. In the limit of a continuous distribution of sites, the form factors $\omega_i(q) \equiv \omega_{ii}(q)$ ($1 \leq i \leq 2$) are easily calculated to be²³:

$$\omega_i(q) = \frac{2N_i}{(qR_i)^2} \left(1 - \frac{J_1(2qR_i)}{qR_i} \right), \quad (5.1)$$

where J_1 denotes the cylindrical Bessel function of first order and all interaction sites are assumed to be equivalent, i.e., edge effects are neglected. This may be a more severe approximation for platelets than for spheres (where the equivalence is exact), or rigid or semiflexible polyelectrolyte chains, but our previous results for the one-component case show that it leads to good agreement with available simulation data¹¹. The correlation

function matrices $\mathbf{H}(q)$ and $\mathbf{C}(q)$ are now 2×2 matrices, and $\mathbf{W}(q)$ is diagonal.

We have solved the PRISM equations for platelet parameters and physical conditions appropriate for a water base drilling mud, made up of large, negatively charged bentonite platelets, (index b), and much smaller, positively charged mixed metal hydroxide platelets (index m). The radii of the two species were taken to be $R_1 = R_b = 10^3$ nm and $R_2 = R_m = 25$ nm; the effective thicknesses were chosen to be $d_b = d_m = 10$ nm, mimicking conditions where the platelets are not fully dispersed and form stacks. The strong screening in water base drilling muds is mainly due to the addition of NaOH (pH=12), and this is modelled by adopting an inverse screening length, $\kappa_D = 1$ nm $^{-1}$. A homogeneous interaction site density on both types of platelets is achieved by imposing $N_b/N_m = R_b^2/R_m^2 = 1600$; in practice $N_b = 30400$ and $N_m = 19$, while surface charge densities were fixed at $\sigma_b = 0.09$ e nm $^{-2}$ and $\sigma_m = 0.9$ e nm $^{-2}$. Examples of bentonite pair distribution functions $g_{bb}(r)$ are shown in Fig. 6. At the two lower clay concentrations, the position of the first peak scales roughly like $\rho_b^{-1/3}$, but at the highest density the peak shifts dramatically towards the origin, a behaviour indicative of a collapse of nearly parallel pairs of bentonite platelets, under the influence of a strong effective attraction, induced by the smaller platelets that appear to "condense" on the surfaces of the bentonite discs. Note that all secondary minima and maxima have disappeared from $g_{pp}(r)$ at the highest density. The corresponding structure factors $S_{bb}(q)$ (minus the fixed intramolecular contribution) are pictured in Fig. 7, together with the results obtained from PRISM for the same bentonite densities, but ten times lower densities of the smaller platelets. The structure factors $S_{bb}(q)$ at the two lower densities show typical liquid-like structure, with a main peak at $q = 2\pi/D_b$, where $D_b \approx \rho_b^{-1/3}$. Increasing ρ_b or adding mixed metal hydroxide shifts the peak toward higher q -values, corresponding to a shorter distance between bentonite platelets. Increasing ρ_m also leads to an enhancement of the small angle ($q \rightarrow 0$) value of $S_{bb}(q)$; a clear central peak appears at intermediate densities, while at the highest densities the amplitude of the central peak appears to diverge, signalling strong concentration fluctuations indicative of platelet aggregation, or spinodal instability reminiscent of the behaviour observed in recent computer simulations of mixtures of oppositely charged spherical particles³⁸. A similar strong small q upturn has been observed experimentally for monodisperse clay suspensions in the gel phase^{39–44}, polyelectrolyte gels⁴⁵ and mixtures⁴⁶, Poly(styrenesulfonate) ion exchange resins⁴⁷, and low ionic strength polyelectrolyte solutions^{48–50}, but the exact physical origin of these large-scale fluctuations for these systems is still under debate.

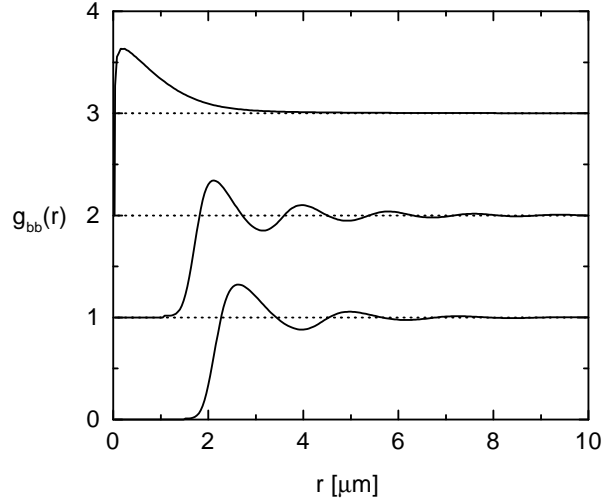


FIG. 6. Pair correlation function $g_{bb}(r)$ for a mixture of large (subscript b) and small, oppositely charged (subscript m) platelets for various densities: $\rho_b = 0.183$ μm^{-3} , $\rho_m = 40$

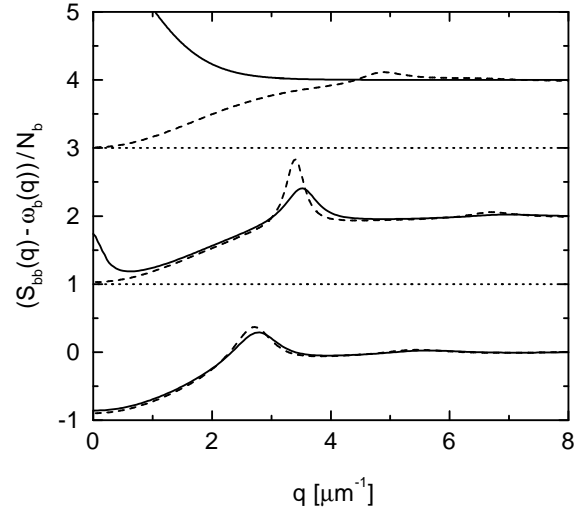


FIG. 7. Platelet structure factor for a mixture of large (subscript b) and small, oppositely charged (subscript m) platelets for various densities: $\rho_b = 0.183$ μm^{-3} , $\rho_{m1} = 4$ μm^{-3} , $\rho_{m2} = 40$ μm^{-3} (top curves); $\rho_b = 0.074$ μm^{-3} , $\rho_{m1} = 1.6$ μm^{-3} , $\rho_{m2} = 16$ μm^{-3} (middle curves); $\rho_b = 0.037$ μm^{-3} , $\rho_{m1} = 0.8$ μm^{-3} , $\rho_{m2} = 8$ μm^{-3} (bottom curves). The dashed and solid lines represent the calculations for ρ_{m1} and ρ_{m2} , respectively. The upper four curves are shifted.

VI. CONCLUSION

We have illustrated the mechanism of mesoscopic particle aggregation induced by oppositely charged polyions on two examples of complex two-component dispersions. The partial "condensation" of the small particles leads to a considerable reduction of the strong Coulomb repulsion between the larger colloidal particles, which may go as far as an effective short-range attraction between the latter. The attraction, and resulting aggregation give rise to a strong enhancement of the long wavelength concentration fluctuations of the large particles, which is well characterized by the small q limit of the corresponding partial structure factor.

While effective attractions have been widely studied theoretically and by simulations in the case of microscopic counterions¹⁷, PRISM has allowed us to extend such studies to cases where the "counterions" are themselves complex objects (semiflexible polyelectrolyte chains or clay platelets). PRISM turns out to be an accurate and flexible tool to tackle highly asymmetric complex systems of charged particles of various shapes, which are beyond the search of present day simulation methodology. The PRISM integral equations provide detailed structural information, in the form of partial, site-site pair distribution functions and structure factors. Thermodynamic properties can then be determined via the energy route, or the compressibility route⁸, but the structural information is not sufficient to give direct access to the equation of state via the viral route, and to the free energy necessary to determine phase diagrams, which requires thermodynamic integration. Work along these lines is in progress, as well as further calculations based on model B for the colloid-polyelectrolyte mixture.

ACKNOWLEDGMENTS

The authors are grateful to Edo Boek for helpful discussions.

¹ For a recent review, see e.g., A. A. Louis, Phil. Trans. Roy. Soc. A **359**, 939 (2001).

² A. Sharma, S. N. Tan, and J. Y. Walz, J. Colloid Interface Sci. **190**, 392 (1997) and **191**, 236 (1997).

³ E. M. Mateescu, C. Jeppesen and P. Pincus, Europhys. Lett. **46**, 454 (1999); R. R. Netz and J. F. Joanny, Macromolecules **32**, 9013 and 9026 (1999).

⁴ E. P. Giannelis, R. Krishamoorti, E. Manias, Adv. Polym. Sci. **138** 107 (1999), and references therein.

⁵ W. M. Gelbart, R. F. Bruinsma, P. A. Pincus and V. A. Parsegian, Physics Today **53**, 38 (2000).

- ⁶ Y. Kojima, A. Usuki, M. Kawasumi, A. Okada, T. Kurauchi, O. Kamigaito, J. Polym. Sci. A **31** 983 (1993).
- ⁷ J. Felixberger in "Recent Advances in oilfield chemistry", Proceedings of the 5th International Symposium on Chemistry in the Oil Industry, P. 84, edited by P. H. Ogden, Roy. Soc. of Chemistry (1998).
- ⁸ J.-P. Hansen and I. R. McDonald, *Theory of Simple Liquids*, 2d edition, (Academic Press), London, (1986).
- ⁹ For a review, see K. S. Schweizer and J. G. Curro, Adv. Chem. Phys. **98**, 1 (1997).
- ¹⁰ L. Harnau and P. Reineker, J. Chem. Phys. **112**, 437 (2000).
- ¹¹ L. Harnau, D. Costa and J.-P. Hansen, Europhys. Lett. **53**, 729 (2001).
- ¹² A. Yethiraj, C. Hall, and R. Dickman, J. Colloid Interface Sci. **151** 102 (1992).
- ¹³ P. G. Khalatur, L. V. Zherenkova and A. R. Khokhlov, J. Phys. II France **7**, 543 (1997).
- ¹⁴ A. P. Chatterjee and K. S. Schweizer, J. Chem. Phys. **109**, 10464 and 10477 (1998).
- ¹⁵ M. Fuchs and K. S. Schweizer, Europhys. Lett. **51**, 621 (2000).
- ¹⁶ P. G. Ferreira, M. Dymitrowska, and L. Belloni, J. Chem. Phys. **113**, 9849 (2000).
- ¹⁷ For a recent review, see J.-P. Hansen and H. Löwen, Ann. Rev. Phys. Chem. **51**, 209 (2000).
- ¹⁸ N. Grønbech-Jensen, K. M. Beardmore and P. Pincus, Physica A, **261**, 74 (1998).
- ¹⁹ E. Allahyarov, H. Löwen and S. Trigger, Phys. Rev. E **57**, 5818 (1998).
- ²⁰ N. Grønbech-Jensen, R. J. Mashl, R. F. Bruinsma and W. M. Gelbart, Phys. Rev. Lett. **78**, 2477 (1997).
- ²¹ L. Sjöström, T. Åkesson and B. Jönsson, Ber. Bunsenges. Phys. Chem. **100**, 889 (1996).
- ²² T. Borukhov, D. Andelman and H. Orland, J. Phys. Chem. B **163**, 5042 (1998).
- ²³ S. Kutter, J.-P. Hansen, M. Sprik and E. Boek, J. Chem. Phys. **112**, 311 (2000).
- ²⁴ P. Warren, J. Chem. Phys. **112**, 4683 (2000).
- ²⁵ For a review of RISM, see D. Chandler in "Studies in Statistical Mechanics", vol. 8, P. 275, edited by J. L. Lebowitz and E. W. Montroll (North Holland), Amsterdam (1982).
- ²⁶ C.-Y. Shew and A. Yethiraj, J. Chem. Phys. **110**, 11599 (1999).
- ²⁷ D. Laria, D. Wu, and D. Chandler, J. Chem. Phys. **95**, 4444 (1991).
- ²⁸ K. S. Schweizer and A. Yethiraj, J. Chem. Phys. **98**, 9053 (1993).
- ²⁹ A. Kovalenko and F. Hirata, J. Chem. Phys. **110**, 10095 (1999); *ibid* **112**, 9463 and 10391 (2000).
- ³⁰ L. Harnau, R. G. Winkler and P. Reineker, J. Chem. Phys. **104**, 6355 (1996).
- ³¹ I. Pagonabarraga and M. E. Cates, Europhys. Lett., **55**, 348 (2001).
- ³² V. Krakoviak, J.-P. Hansen and A. A. Louis, submitted to Europhys. Lett. (2001).
- ³³ J. Rescic and P. Linse, J. Phys. Chem. B. **104**, 7852 (2000).
- ³⁴ G. Manning, J. Chem. Phys. **51**, 924 (1969).
- ³⁵ Y. Levin, M. C. Barbosa and M. N. Tamashiro, Europhys. Lett. **41**, 123 (1998).

- ³⁶ P. G. Bolhuis, A. A. Louis, J.-P. Hansen, and E. J. Meijer, J. Chem. Phys. **114**, 4296 (2001).
- ³⁷ T. Hofmann, R. G. Winkler, and P. Reineker, J. Chem. Phys. **114**, 10181 (2001).
- ³⁸ P. Linse and V. Lobaskin, Phys. Rev. Lett **83**, 4208 (1999).
- ³⁹ M. Morvan, D. Espinat, J. Lambard and Th. Zemb, Colloid Surf. A **82**, 193 (1994).
- ⁴⁰ F. Pignon, A. Magnin, J.-M. Piau, B. Cabane, P. Lindner and O. Diat, Phys. Rev. E **56**, 3281 (1997).
- ⁴¹ A. Mourchid and P. Levitz, Langmuir **57**, 4887 (1998).
- ⁴² M. Kroon, W. L. Vos, and G. H. Wegdam, Phys. Rev. E **57**, 1962 (1998).
- ⁴³ J. M. Saunders, J. W. Goodwin, R. M. Richardson, and B. Vincent, J. Phys. Chem. B **103**, 9211 (1999).
- ⁴⁴ D. Bonn, H. Kellay, H. Tanaka, G. Wegdam, and J. Meunier, Langmuir **15**, 7534 (1999).
- ⁴⁵ F. Schosseler, R. Skouri, J. P. Munch, and S. J. Candau, J. Phys. II France **4**, 1221 (1994).
- ⁴⁶ D. P. Norwood, M. Benmouna, and W. F. Reed, Macromolecules **29**, 4293 (1996).
- ⁴⁷ J. R. C. van der Maarel, W. Jesse, M. E. Kuil, and A. Lapp, Macromolecules **29**, 2039 (1996).
- ⁴⁸ S. Förster, M. Schmidt, M. Antonietti, Polymer **31**, 781 (1990).
- ⁴⁹ F. Boue, J. P. Cotton, A. Lapp, G. Jannink, J. Chem. Phys. **101**, 2562 (1994).
- ⁵⁰ B. D. Ermi and E. J. Amis, Macromolecules **31**, 7378 (1998).